Aerodynamic Nacelle Shape Optimization for NAL's Experimental Airplane

Yoshikazu Makino and Toshiyuki Iwamiya
National Aerospace Laboratory
7-44-1 Jindaijihigashi-machi, Chofu, Tokyo 182-8522, JAPAN

Zhong Lei
VINAS Co., Ltd.
1-18-35 Edobori, Nishi, Osaka, Osaka 550-0002, JAPAN

Abstract

The numerical simulation of a Mach 2.0 scaled supersonic experimental airplane is conducted with the consideration of the integration between airframe and engine nacelles. A three-dimensional Euler CFD code with an overset-grids technique is adopted for solving the flow-field around a complex airplane configuration. The calculated pressure distributions are compared with wind tunnel test data and show good agreement with them. The aerodynamic design tool which combines the CFD code with an optimization technique for drag minimization is developed. At first, it is applied to an axisymmetrical body in order to validate this design tool. The result shows that the optimized body geometry agrees well with the Sears-Haack body. Next, it is applied to two bodies under a wing-body configuration. The pressure drag of the optimized configurations is about 9 percent lower than that of the Sears-Haack body maintaining their final volumes.

Introduction

National Aerospace Laboratory (NAL) of Japan started a scaled supersonic experimental airplane program which we call NEXST (National Experimental Supersonic Transport)[1] in 1996 in order to establish advanced technologies including a sophisticated CFD-based total design tool for the next generation supersonic civil transport. In this program, at first we will conduct flight tests of an un-manned non-powered experimental airplane in 2002. This airplane was designed at Mach 2.0 adopting a NAL's original aerodynamic design technology together with CFD prediction[2]. Its design concepts for a high lift/drag ratio are a cranked arrow wing, a modulated warp, an area-ruled configuration and a natural laminar flow wing. In order to develop a CFD-based total aerodynamic design tool for a complete airplane configuration, a jet-powered experimental airplane will be designed as a successor of the non-powered airplane. Considerations of airframe/nacelle integration are important in the design process of this jet-powered airplane.

Numerical Simulation Method

In order to simulate the flow around a complex airplane configuration, an overset-grids technique is adopted in our study. The airplane configuration which is a half configuration in computational space is divided into five components; wing-body, engine nacelle, diverter, horizontal tail and vertical tail. The grids which are independently generated around each component are overlapped. Figure 1 shows the computational grids generated around the non-powered experimental airplane configuration with an axisymmetrical engine nacelle. This simple flow-through nacelle configuration is an experimental model configuration used in our wind tunnel tests. A CFD code which is based on three-dimensional Euler equations is used to solve the flow-field around the airplane. The numerical method is an implicit finite difference scheme. The diagonalized ADI scheme which utilizes an upwind flux-split technique is used for the implicit left-hand-side, and a higher-order upwind scheme based on TVD scheme by Chakravarthy and Osher[3] is applied to the explicit right-hand-side. Communications among the overset-grids are accomplished by interpolations of the independent variables at grid boundaries[4]. Figure 2 shows the calculated surface pressure contours of the airplane in the case of angle-of-attack 2° at Mach 2.0. It is shown in the figure that two strong shocks are generated from the nacelles and diverters on each side of the wing. These shocks interact under the

centerline of the airplane and generate high pressure region on the lower wing surface. Figure 3(a) to 3(c) show the fuselage and wing surface pressure distributions compared with the experimental data at spanwise location η=0.0 (fuselage center line), η=0.3 (nacelle center line) and η=0.5, respectively. At η=0.0 and η=0.3, the calculated pressure distributions and the experimental data show good agreement. At η=0.5, there are two pressure peaks on the lower surface of the wing which are due to the shocks from the nacelle and diverter. The pressure rise due to the nacelle in the calculated pressure distribution is located more rearward than that in the experimental data. A grid sensitivity analysis will be necessary in order to clarify whether this discrepancy is due to the viscous effects which cannot be considered by our Euler CFD code.

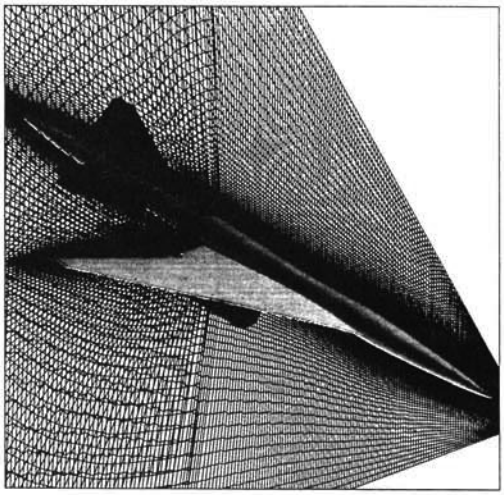

Figure 1: Overset grids.

Figure 2: Surface pressure contours.

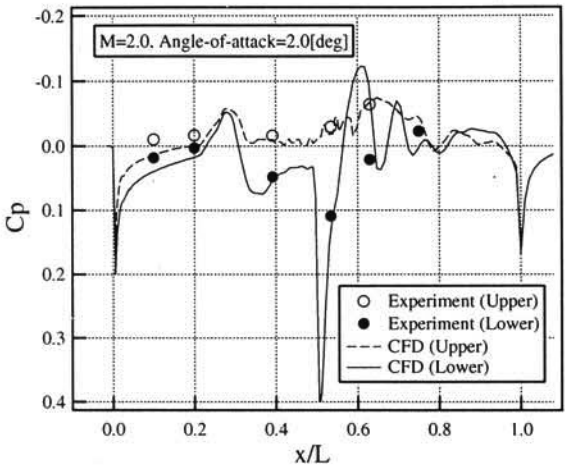

(a) $\eta = 0.0$.

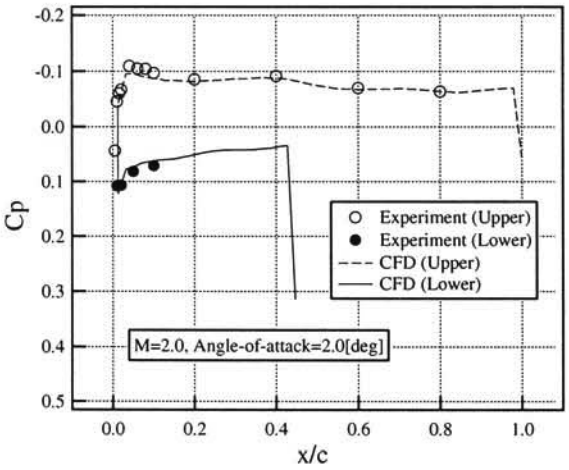

(b) $\eta = 0.3$.

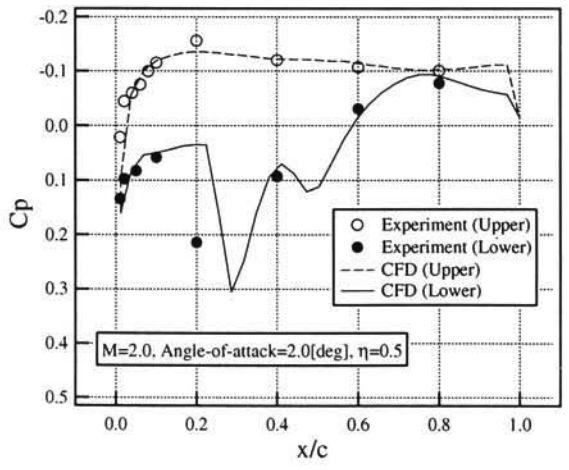

(c) $\eta = 0.5$.

Figure 3: Calculated pressure distributions compared with experimental data.

Aerodynamic Design Method

In order to reduce interaction drag between airframe and engine nacelles, position and shape optimization tools for designing the propulsion system are needed. The design tool which combines the CFD code with an optimization technique is developed in our study. A quasi-Newton optimization method based on a conjugate gradient method is adopted as an optimization technique. At first, it is applied to an axisymmetrical body configuration to minimize the pressure drag as a sample demonstration. The object function to be minimized through the optimization is:

$$I = \frac{C_{Dp} + K \times \left(\frac{V-V_0}{V_0}\right)^2 \times H(V_0 - V)}{C_{Dp_0}} \quad (1)$$

where C_{Dp} and V are a pressure drag coefficient and a volume of an axisymmetrical body, respectively. The subscript 0 means the initial value. The function $H(x)$ is the Heaviside step function which replies 1 when x has a positive value and replies 0 when x is less than 0. The quantity K is a coefficient of a penalty function in order to keep the body volume no less than that of an initial geometry. This penalty function coefficient K is 5 in this case. The initial axisymmetrical body geometry shown in Figure 4 is modified by adding radial perturbations whose axial distribution is defined by a Bezier curve controlled by 7 points including fixed two points at nose and tail of the body. The radial coordinates of the other 5 points are used as design variables in the optimization process.

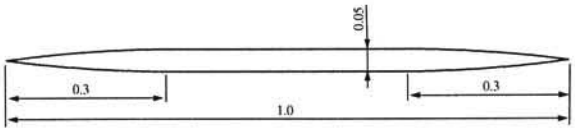

Figure 4: Initial axisymmetrical body geometry.

One design cycle of the quasi-Newton optimization method is composed of two processes: gradient calculation of the object function and line minimization in the direction which is conjugate to the calculated steepest direction. As for the gradient calculation process, two methods are used in this study. One method is a finite difference method and another is an adjoint method[5]. In the finite difference method, the gradients of the object function to all design variables are calculated by adding a small perturbation to every design variable and evaluating the object function by CFD one by one. Therefore the number of CFD calculations is the same as that of the design variables in this process. The general formulation of the adjoint method is shown in Reference 5. The object function is defined by the aerodynamic properties which are functions of the flow-field variables(q) and the physical location of the boundary($\mathcal{F}$).

$$I = I(q, \mathcal{F}) \quad (2)$$

A change in $\mathcal{F}$ results in a change

$$\delta I = \left[\frac{\partial I}{\partial q}\right]_{\mathrm{I}}^T \delta q + \left[\frac{\partial I}{\partial \mathcal{F}}\right]_{\mathrm{II}}^T \delta \mathcal{F} \quad (3)$$

in the object function, where the subscript I represents $\delta\mathcal{F} = 0$ and the subscript II means $\delta q = 0$. The governing equations of the flow-field and their variations are

$$R(q, \mathcal{F}) = 0 \quad (4)$$

$$\delta R = \left[\frac{\partial R}{\partial q}\right]_{\mathrm{I}} \delta q + \left[\frac{\partial R}{\partial \mathcal{F}}\right]_{\mathrm{II}} \delta \mathcal{F} = 0 \quad (5)$$

Next, introducing a Lagrange Multiplier ψ, we have

$$\begin{aligned} \delta I &= \delta I - \psi^T \delta R \\ &= \left\{\left[\frac{\partial I}{\partial q}\right]^T - \psi^T \frac{\partial R}{\partial q}\right\}_{\mathrm{I}} \delta q \\ &\quad + \left\{\left[\frac{\partial I}{\partial \mathcal{F}}\right]^T - \psi^T \frac{\partial R}{\partial \mathcal{F}}\right\}_{\mathrm{II}} \delta \mathcal{F} \end{aligned} \quad (6)$$

Choosing ψ to satisfy the following adjoint equations

$$\left[\frac{\partial I}{\partial q}\right]_{\mathrm{I}}^T = \psi^T \left[\frac{\partial R}{\partial q}\right]_{\mathrm{I}} \quad (7)$$

the coefficient of δq becomes zero and we find

$$\begin{aligned} \delta I &= \mathcal{G} \delta \mathcal{F} \\ \mathcal{G} &\equiv \left[\frac{\partial I}{\partial \mathcal{F}}\right]_{\mathrm{II}}^T - \psi^T \left[\frac{\partial R}{\partial \mathcal{F}}\right]_{\mathrm{II}} \end{aligned} \quad (8)$$

Here, the variation of the object function δI is independent of δq. Therefore only one calculation of the adjoint equations is enough to obtain the gradients of the object function. Figure 5 shows the adjoint gradients compared with the finite difference gradients. Good agreements are shown between both methods.

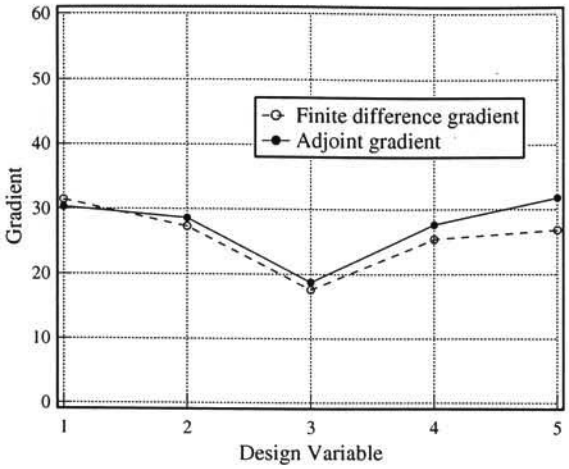

Figure 5: Comparison of gradients.

Figure 6(a) shows the optimized body shapes which are obtained by using both gradient estimation methods compared with the initial geometry. They are also compared with the Sears-Haack body whose volume equals to that of the initial geometry. Both optimized geometries agree with the Sears-Haack body. Figure 6(b) to 6(d) show the convergence histories of the object function, the pressure drag coefficient and the volume of the body with respect to the number of CFD calculations. In Figure 6(b), it is shown that the object function by the finite difference gradient goes down every step in the optimization process. This step shape represents the two processes in one design cycle: the finite difference gradients are calculated in the flat part of the step and then the object function goes down by the line minimization process. It is shown that the object function which is obtained by using the adjoint gradients converges at about 15th CFD calculation while one obtained by using the finite difference gradients converges after 90 CFD calculations. Including the computational costs for calculating the adjoint equations every design cycle, the total computational cost of the adjoint method is much smaller than that of the finite difference method. This merit of the adjoint method increases when the number of the design variables becomes large. As shown in Figure 6(c), the pressure drag coefficients of both optimized geometries are about the same as that of the Sears-Haack body. The body volume of both optimized geometries are, however, about 0.7 percent smaller than that of the Sears-Haack body. These results suggest that the penalty function coefficient K, which is 5 in this case, should be larger in order to keep the initial volume.

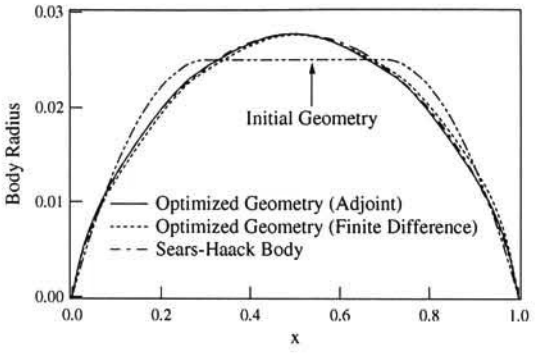

(a) Optimized geometries.

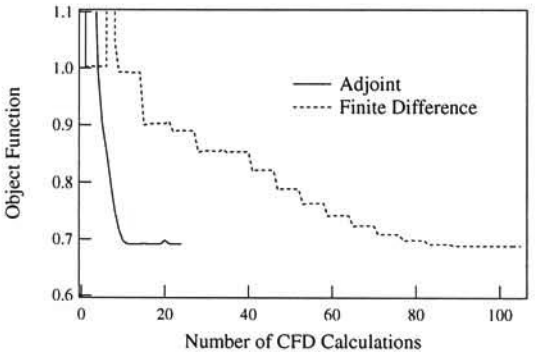

(b) Object function.

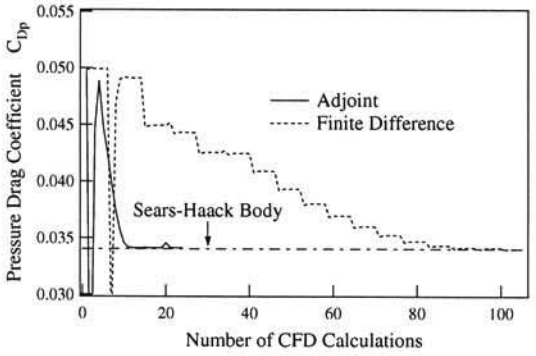

(c) Pressure drag coefficient.

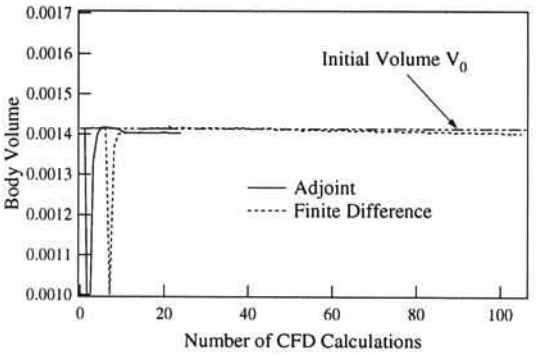

(d) Body volume.

Figure 6: Optimization results for the axisymmetrical body.

Design Results

Next, the design tool which uses the adjoint gradients is extended to a complex airplane geometry. In Reference 6, the adjoint method is applied to a complex airplane geometry with a multi-block technique. In this work, it is extended to be used with an overset-grids technique and applied to two bodies under a wing-body configuration as shown in Figure 7. The object function of the design cycle is the same as stated in equation (1) in which C_{Dp} is the pressure drag coefficients of two bodies. The penalty function coefficient K is 50 in this case. The Sears-Haack body is selected as an initial geometry. The calculated pressure contours on the wing-body configuration with these initial axisymmetrical bodies are also shown in Figure 7. Figure 8 shows the calculated pressure coefficient distributions along the upper, inner, lower, outer side lines on the initial bodies. In this figure, there is a pressure rise due to the nose shock in the front part of every pressure distribution. In the upper-side line, a pressure peak is shown at about $x = 0.25$ which is due to the reflected shock from the lower surface of the wing. This reflected shock generates pressure increases in the inner and outer side lines, too. In the inner side line, another pressure peak is shown at about $x = 0.6$ which is due to the shock from another body nose. Therefore, two shape modification methods are used in this design process. The first method is axisymmetrical modification which is the same as the single body case. Another method is non-axisymmetrical modification in which only the upper and inner side radius distributions are changed while the lower and outer side ones are fixed. In this case the number of design variables are 10 in which each 5 controlling points are distributed on the upper and inner side line, respectively. These design variables control Bezier curves as stated in previous section.

The design results are shown in Figure 9. Figure 9(a) shows the body radius distributions of the optimized body geometries. In the case of non-axisymmetrical modification, the upper-side geometry becomes flatter in the front part in order to reduce the drag component of the high pressure force due to the reflected shock. Similarly, the location of the maximum radius of the inner side geometry goes forward in order to increase the thrust component of the high pressure force due to the shock from another body nose. Figure 9(b) to 9(d) show the convergence histories of the object function, the pressure drag coefficient and the volume of the body, respectively, with respect to the number of CFD calculations. Both object functions converge after about 17 CFD calculations. The final pressure drag coefficient of the non-axisymmetrical body is about 9.4 percent lower than that of the Sears-Haack body. This drag coefficient is lower than that of the axisymmetrical optimized body which is about 6.7 percent lower than that of the Sears-Haack body. The final volumes of both optimized bodies are almost the same as the initial volume as shown in Figure 9(d).

This is just a test case for designing nacelle shapes and the design method developed here will be soon applied to the flow-through nacelles shown in Figure 2 in our future work.

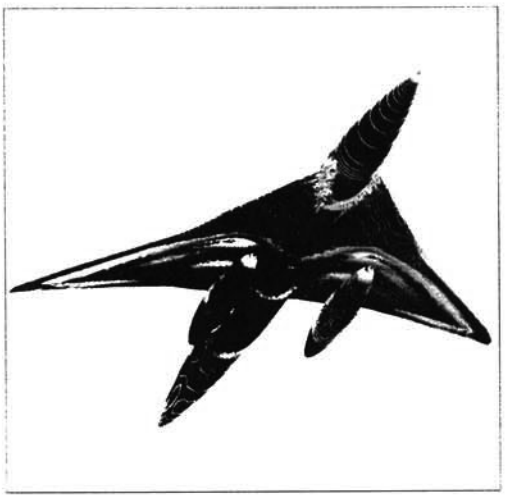

Figure 7: Two axisymmetrical bodies under the wing-body configuration.

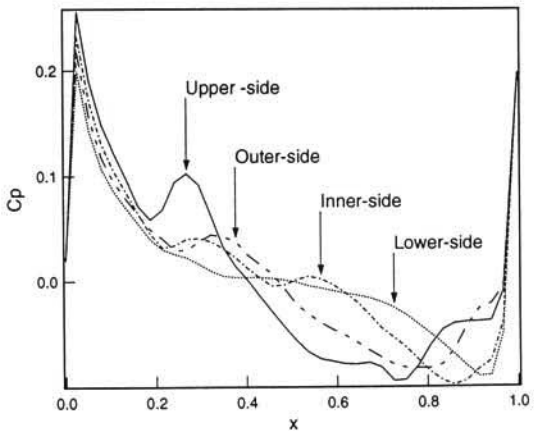

Figure 8: Pressure coefficient distributions on the Sears-Haack body.

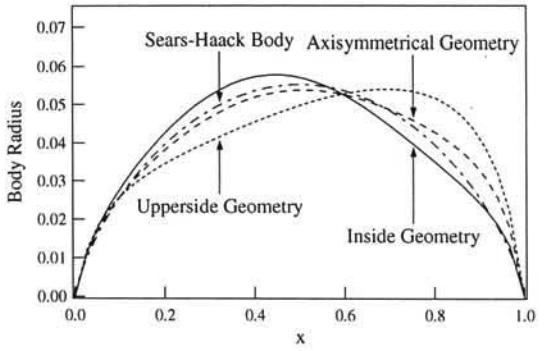

(a) Optimized geometries.

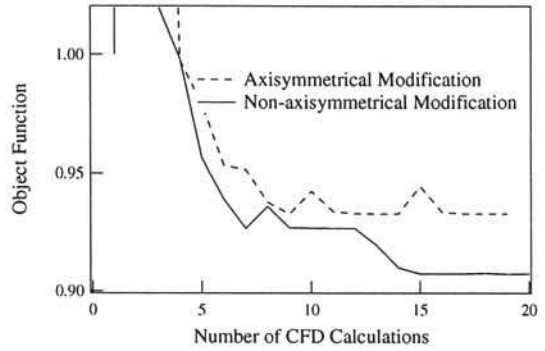

(b) Object function.

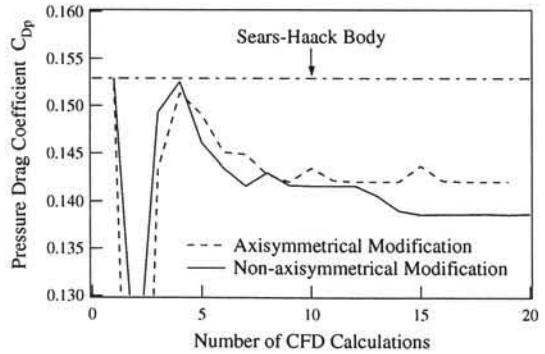

(c) Pressure drag coefficient.

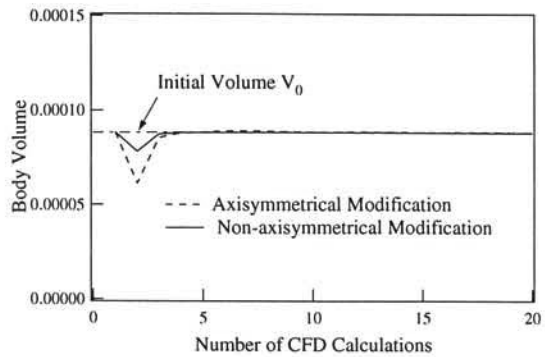

(d) Body volume.

Figure 9: Optimization results for two bodies under the wing-body configuration.

Conclusions

The numerical simulation of a complex airplane geometry is conducted by using the three-dimensional Euler CFD code with an overset-grids technique. The calculated pressure distributions show good agreement with the experimental data. The aerodynamic design tool is developed by combining the CFD code with an optimization technique which utilizes either finite difference gradients or adjoint gradients. The results of its application to an axisymmetrical body show that the pressure drag coefficients of the optimized bodies are about the same as the Sears-Haack body and the convergence of the design cycle of the adjoint method is faster than that of the finite difference method. The design tool is applied to two bodies under a wing-body configuration. The results indicate that in the specific flow situation including shock interactions, the Sears-Haack body is not a minimum drag configuration. The pressure drag coefficient of the non-axisymmetrical optimized body is lower than that of the axisymmetrical optimized body in such a flow situation.

Acknowledgement

The authors express their sincere gratitude to Mr.Yuichi Shimbo and Mr.Masayoshi Noguchi for providing the experimental data.

References

1. Sakata, K., "Supersonic Research Program in NAL, Japan," 1st International CFD Workshop for Super-Sonic Transport Design, pp.1-4, 1998.

2. Shimbo, Y., Yoshida, K., Iwamiya, T., Takaki, R. and Matsushima, K., "Aerodynamic Design of the Scaled Supersonic Experimental Airplane," 1st International CFD Workshop for Super-Sonic Transport Design, pp.62-67, 1998.

3. Chakravarthy, S.R. and Osher, S., "A New Class of High Accuracy TVD Schemes for Hyperbolic Conservation Laws," AIAA paper 85-0363, 1985.

4. Benek, J.A., Buning, P.G. and Steger, J.L., "A 3-D Chimera Grid Embedding Technique," AIAA paper 85-1523, 1985.

5. Jameson, A., "Optimum Aerodynamic Design Using CFD and Control Theory," AIAA paper 95-1729-CP, 1995.

6. Reuther, J., Jameson, A., Farmer, J., Martinelli, L, and Saunders, D., "Aerodynamic Shape Optimization of Complex Aircraft Configurations via an Adjoint Formulation," AIAA paper 96-0094, 1996.